The Self-Consistent Charge Density Functional Tight Binding Method Applied to Liquid Water and the Hydrated Excess Proton: Benchmark Simulations

C. Mark Maupin,[†] Bálint Aradi,[‡] and Gregory A. Voth*[,†,§]

Department of Chemistry, James Franck Institute, and Computation Institute, University of Chicago, 5735 South Ellis Avenue, Chicago, Illinois, 60637, Center for Biophysical Modeling and Simulation and Department of Chemistry, University of Utah, 315 South 1400 East, Room 2020, Salt Lake City, Utah 84112, and Bremen Center for Computational Materials Science, University Bremen, Bremen, Germany 283359

Received: February 3, 2010; Revised Manuscript Received: March 19, 2010

The self-consistent charge density functional tight binding (SCC-DFTB) method is a relatively new approximate electronic structure method that is increasingly used to study biologically relevant systems in aqueous environments. There have been several gas phase cluster calculations that indicate, in some instances, an ability to predict geometries, energies, and vibrational frequencies in reasonable agreement with high level ab initio calculations. However, to date, there has been little validation of the method for bulk water properties, and no validation for the properties of the hydrated excess proton in water. Presented here is a detailed SCC-DFTB analysis of the latter two systems. This work focuses on the ability of the original SCC-DFTB method, and a modified version that includes a hydrogen bonding damping function (HBD-SCC-DFTB), to describe the structural, energetic, and dynamical nature of these aqueous systems. The SCC-DFTB and HBD-SCC-DFTB results are compared to experimental data and Car−Parrinello molecular dynamics (CPMD) simulations using the HCTH/120 gradient-corrected exchange-correlation energy functional. All simulations for these systems contained 128 water molecules, plus one additional proton in the case of the excess proton system, and were carried out in a periodic simulation box with Ewald long-range electrostatics. The liquid water structure for the original SCC-DFTB is shown to poorly reproduce bulk water properties, while the HBD-SCC-DFTB somewhat more closely represents bulk water due to an improved ability to describe hydrogen bonding energies. Both SCC-DFTB methods are found to underestimate the water dimer interaction energy, resulting in a low heat of vaporization and a significantly elevated water oxygen diffusion coefficient as compared to experiment. The addition of an excess hydrated proton to the bulk water resulted in the Zundel cation ($H_5O_2^+$) stabilized species being the stable form of the charge defect, which diffuses at a rate similar to the underlying water diffusion. These SCC-DFTB results differ significantly from other existing computational descriptions of the hydrated excess proton in water, as well as from the available experimental data.

1. Introduction

The ability to accurately and efficiently model bulk water as well as the hydrated excess proton in water is a high priority for molecular simulations and one that has seen significant advances in the past decade. While methods that evaluate energy and forces from quantum mechanics (QM) are ideal, the computational cost of these high level calculations has generally made them computationally intractable for systems larger than small gas phase clusters. Car−Parrinello molecular dynamics[1] (CPMD) is an approach capable of treating the condensed phase, but these simulations are restricted to relatively small numbers of water molecules and short time scales due to their large computational cost.[2] Therefore, the descriptions of bulk water solutions and biomolecular systems have generally been treated by computationally simpler and more efficient empirical force field methods.[3−5] These empirical models, while able to simulate large system sizes with long-range electrostatics and periodic boundary conditions (PBCs), may be hindered by potential inaccuracies in describing certain physical properties of aqueous systems due to the simplicity of the underlying functional forms. One alternative approach is therefore to develop models that retain certain benefits of QM methods such as chemical reactivity while possessing the ability to simulate larger systems for relevant time scales.[6,7]

To address the system size and time scale issues that make using high level QM methods computationally intractable, the QM Hamiltonian may be simplified to allow for an increase in computational speed. Such a simplification of course comes at the expense of overall accuracy, making it critical to assess the magnitude of the inaccuracies. To this end, the approximate quantum mechanical self-consistent charge density functional tight binding (SCC-DFTB) method[8−16] has shown promise in its ability to reproduce the geometries, energies, and vibrational frequencies of certain gas phase molecules and clusters compared to higher level QM methods.[10,16−18] This success is not, however, universal, as demonstrated in the companion paper, ref 19. The SCC-DFTB method has also been extensively applied to study proton transfer in biomolecular systems.[15,20−28] (The SCC-DFTB method is referred to here as approximate instead of semiempirical due to the DFTB parameters being fit mostly against ab initio calculations.)

While the SCC-DFTB method has been claimed to reasonably reproduce certain cluster geometries and energies, it has received little validation for its ability to reproduce bulk water properties[29] and no validation to date for the properties of the hydrated excess proton in water. The latter is of particular relevance given the

* Corresponding author. E-mail: voth@hec.utah.edu.
[†] University of Utah.
[‡] University Bremen.
[§] University of Chicago.

10.1021/jp1010555
Published on Web 04/28/2010

growing use of the SCC-DFTB method to study proton solvation and transport in biomolecular systems.[15,16,20−28] Therefore, a greater degree of validation of the SCC-DFTB method for simpler aqueous systems (without and with the excess proton) is clearly desirable.

The focus of this manuscript is to evaluate the accuracy of the SCC-DFTB method and a specific parametrization set (mio-0-1) for describing the structural, energetic, and dynamical properties of neat bulk water, as well as the hydrated excess proton in water. The simulations of neat bulk water provide a baseline for the underlying SCC-DFTB aqueous environment and are also compared to previous bulk water SCC-DFTB simulations utilizing a linear scaling divide and conquer method.[29] In the current simulations, no such approximation was used, as PBCs were utilized in conjunction with Ewald summation long-range electrostatics, calculated with the supercell method, in an effort to more realistically simulate the bulk properties of all systems. A detailed analysis of the neat bulk water and the excess proton in water reveals significant inaccuracies in the SCC-DFTB method as it presently stands. These results may also point to possible areas of improvement for the underlying method and/or parametrization set. The companion paper[19] presents a similarly detailed analysis of the SCC-DFTB method for two important benchmark protonated water clusters.

2. Methods

2.1. SCC-DFTB. ***2.1.1. SCC-DFTB Electronic Structure Method.*** The approximate SCC-DFTB method is based on a second-order expansion of the Kohn−Sham total energy with respect to the charge density fluctuations

$$E_{\text{total}}^{\text{SCCDFTB}} = \sum_{i\mu v} c_\mu^i c_v^i H_{\mu v}^0 + \frac{1}{2}\sum_{\alpha\beta} \Delta q_\alpha \Delta q_\beta \gamma_{\alpha\beta} + E_{\text{rep}} \tag{1}$$

where c_μ^i and c_v^i are the wave function expansion coefficients, $H_{\mu v}^0$ are the Hamiltonian matrix elements, Δq_α and Δq_β are the charge fluctuation terms for atoms α and β, and E_{rep} is an approximation of the short-range repulsion term.[8−16] In the original SCC-DFTB method, the $\gamma_{\alpha\beta}$ function is determined by

$$\gamma_{\alpha\beta} = \frac{1}{r_{\alpha\beta}} - S_{\alpha\beta} \tag{2}$$

were $r_{\alpha\beta}$ is the distance between atom α and β and $S_{\alpha\beta}$ is the short-range correction term between the nuclei of atom α and β. Subsequently, it was found that incorporating a damping function on the $\gamma_{\alpha\beta}$ term for atomic pairs involving hydrogen increased the accuracy of describing hydrogen bonds.[16] The $\gamma_{\alpha\text{H}}$ term for the hydrogen bonding damping function SCC-DFTB (HBD-SCC-DFTB) is defined as

$$\gamma_{\alpha\text{H}} = \frac{1}{r_{\alpha\text{H}}} - S_{\alpha\text{H}} \times \exp\left[-\left(\frac{U_\alpha + U_\text{H}}{2}\right)^\zeta r_{\alpha\text{H}}^2\right] \tag{3}$$

where U_α and U_H are the atomic Hubbard parameters, which are related to the chemical hardness of atom α and a corresponding hydrogen and ζ is determined by fitting to hydrogen bonding energies for select clusters from high level QM calculations. It is noted that alternative methods such as charge damping or charge scaling have also been utilized in an empirical potential for water in an effort to more accurately describe hydrogen bonding characteristics.[30]

The results of a SCC-DFTB calculation depend on both the method and the chosen underlying parametrization set. In contrast to most semiempirical methods, the method and the parametrization set are completely separate in DFTB. The underlying parametrization set used in this manuscript is the mio-0-1 set which is a pairwise parametrization based on the DF-based (two-center) TB approach as indicated in ref 8. All comparisons between the methods, original SCC-DFTB and HBD-SCC-DFTB, are made in light of a similar underlying parametrization set. Therefore, differences that arise are predominately due to the method while underlying accuracies/deficiencies may be due to either the method approximations or parametrization set.

2.1.2. SCC-DFTB Simulation Setup. The bulk water system was created by simulating 128 modified TIP3P[31] classical water molecules for 500 ps of molecular dynamics (MD) in the constant NVE ensemble followed by 500 ps in the constant NPT ensemble.[32] The water system used periodic boundary conditions with long-range Coulombic interactions calculated by Ewald summation, while short-ranged nonbonded interactions and forces were subject to a 7 Å cutoff.[33] The MD simulations were carried out at 300 K and used an MD time integration step within the Verlet integrator of 1 fs. During the constant NPT ensemble, the simulations were run at 1 atm and utilized the Nosé−Hoover thermostat.[34] The pre-equilibration simulations were completed using the DLPOLY2.15 software package and were done in duplicate.[35] The NPT pre-equilibration simulations resulted in box dimensions of $15.8 \times 15.8 \times 15.8$ Å^3 and a corresponding density of $\rho = 0.97$ g/mL ($\exp \rho = 0.997$ g/mL). These classically pre-equilibrated boxes of water were then used as the starting configurations for two 60 ps equilibration constant NVT ensemble simulations in the DFTB+ code.[36] The latter simulations were conducted at a temperature of 300 K using an Anderson thermostat, an integration time step of 1 fs, and SCC convergence criteria of 10^{-6} atomic units. After equilibration, the systems were subjected to a production run of 60 ps in the constant NVE ensemble. The electrostatics for all of the DFTB+ simulations were treated by the supercell sampling using the $2 \times 2 \times 2$ Monkhorst−Pack[37] scheme. The bulk water simulations were carried out, in duplicate, for both the original SCC-DFTB method and the modified HBD-SCC-DFTB method, for a total of four independent simulations. In the HBD-SCC-DFTB simulations, ζ in the modified γ function was set to 4.5; a value of 4.88 was also simulated to test system dependence on ζ but did not yield significant differences. Therefore, only the results for $\zeta = 4.5$ are reported. All SCC-DFTB simulations used the mio-0-1 parametrization set.[8]

For the creation of the excess hydrated proton system, the pre-equilibrated water box was modified by the addition of an excess proton. The resulting system was then equilibrated as described above. In the excess proton system, a neutralizing background charge was used in lieu of an explicit counterion so as to better model high dilution conditions. The production simulation for the excess proton system was conducted as stated above with the exception that the excess proton system production runs were 50 and 80 ps for the SCC-DFTB and HBD-SCC-DFTB methods, respectively. As with the bulk water simulations, the excess proton simulations were done in duplicate (two independent trajectories) for both the original SCC-DFTB and the HBD-SCC-DFTB method.

2.2. CPMD. ***2.2.1. CPMD Simulation Setup.*** The CPMD simulation system in the present work consisted of 128 water

molecules plus an additional proton for the excess hydrated proton systems. The simulations were conducted in a periodic box of dimensions 15.6 × 15.6 × 15.6 Å^3. As done previously,[38] the CPMD system coordinates were taken from an equilibrated MD simulation using an empirical water force field developed from a force matching of CPMD data.[39] The CPMD systems were then equilibrated for 8 ps using a simple velocity rescaling method to maintain a temperature of 300 K. The production runs were then simulated in the constant NVE ensemble for 27 and 35 ps, as two independent runs. The CPMD simulations were completed using the CPMD code, version 3.5,[40,41] and used a plane-wave basis set with an 80 Ry cutoff, Troullier−Martins pseudopotentials[42] for nuclear−electron interactions, and the HCTH/120 exchange-correlation functional[43] for the electron−electron interactions. The HCTH functional was used due to an apparent improved description of liquid water.[38,43−45] The systems were integrated with a time step of 0.073 fs and a fictitious electronic mass of 340 au, which has been shown to give better converged structural and dynamical properties.[38,46] The neat bulk water system was not simulated for the CPMD method; the structural and dynamical quantities were therefore taken from the excess proton systems. Water molecules beyond the third solvation shell of the protonated water molecule with the most hydronium ion character were used to evaluate the reported properties.

For the gas phase dimer calculations reported later, the dimer of interest was inserted into a periodic box of dimensions 20 × 20 × 20 Å^3 and several single point energy calculations were conducted on the input geometries. The box size dimensions were determined by incrementally increasing the side length until the resulting energy values converged, which ensures that the periodic images are sufficiently separated.

3. Results and Discussion

To accurately simulate biological systems, one must have the capability to reproduce the basic structural, energetic, and dynamical properties of the underlying aqueous environment. This in principle requires that the water model reproduce, as closely as possible, the experimentally determined bulk water properties. While accurately reproducing cluster geometries, energies, and vibrational frequencies is also valuable, the ability to reproduce bulk properties is clearly more important when simulating fully hydrated complex systems. The need to properly simulate bulk properties is vital when defects, such as an excess proton, are incorporated. It is therefore fundamentally important to validate the underlying water model and its influence on defects, such as the hydrated excess proton, before proceeding to the incorporation of defects into more complex systems, due to the obvious dependence of the defects on the underlying water model. Therefore, the structural, energetic, and dynamical properties of neat bulk water and the excess proton in bulk water are simulated using the original SCC-DFTB, HBD-SCC-DFTB, and CPMD methods in order to validate the underlying theoretical models.

3.1. Bulk Water. ***3.1.1. Structural Properties.*** To evaluate the accuracy of the SCC-DFTB method for simulating neat bulk water, the radial distribution functions (RDF or $g(r)$) and three-dimensional (3-D) iso-density contour surfaces are used to quantify the structural properties. The dimer interaction surfaces and the heat of vaporization are used to evaluate the energetic features, while the water oxygen diffusion coefficient is used to probe the dynamical properties. The RDFs for oxygen−oxygen ($g_{OO}(r)$, Figure 1A), oxygen−hydrogen ($g_{OH}(r)$, Figure 1B), and hydrogen−hydrogen ($g_{HH}(r)$, Figure 1C) were calculated and

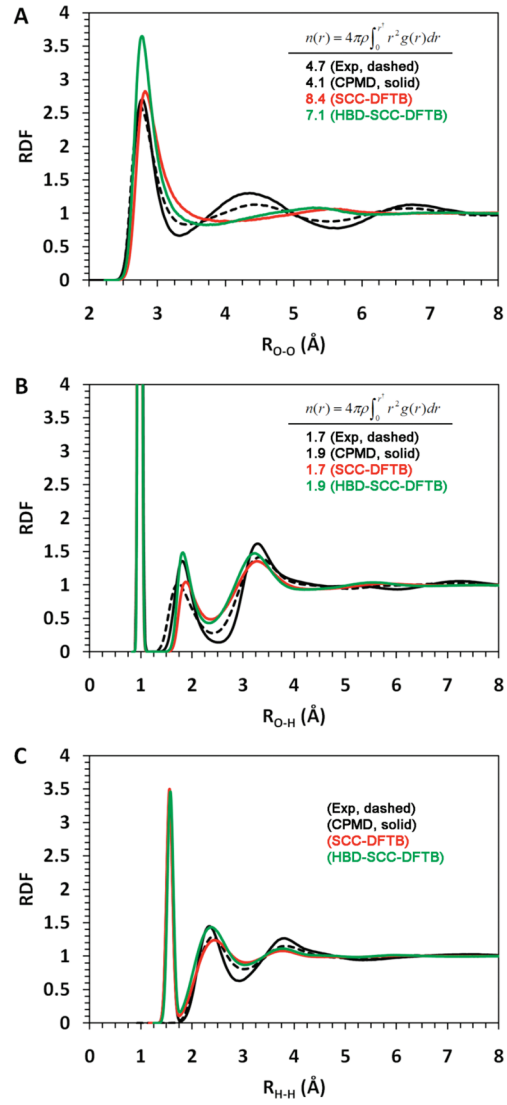

Figure 1. Bulk water radial distribution functions for oxygen−oxygen (A), oxygen−hydrogen (B), and hydrogen−hydrogen (C). Each plot contains experimental data from ref 47 (black dashed), CPMD simulation data (black solid), and SCC-DFTB data from trajectories using the original (red solid) and HBD method (green solid). The number of water oxygens in the first solvation shell for the $g_{OO}(r)$ and the number of hydrogens in the first solvation shell for the $g_{OH}(r)$ are given for each data set in parts A and B, respectively.

compared to experimental[47] data in addition to the results of CPMD simulations. It is clear from Figure 1A that, although the SCC-DFTB and the HBD-SCC-DFTB methods reproduce some general trends seen in the experimental data and CPMD simulations, both have considerable difficulty reproducing even the qualitative behavior of the RDF, especially after the first solvation shell. In fact, the SCC-DFTB models do not possess what would be described as a pronounced second or third solvation shell. In addition, when the experimental data and CPMD simulations indicate a density depletion between the second and third solvation shell, the SCC-DFTB data has a density maxima, showing that the SCC-DFTB results give an incorrect structure for liquid water. The first peak in $g_{OO}(r)$ for the original SCC-DFTB method also indicates that the oxygen−oxygen separation between the central water and the first solvation shell is slightly elongated compared to experimental data. The incorporation of the HBD term, however, has the effect of decreasing this oxygen−oxygen distance to a value in good agreement with experiment and CPMD simulations.

The incorporation of the HBD term also narrows the first solvation peak and shifts the first density depletion from 4.07 to 3.72 Å, but it creates a first peak in the RDF that is clearly too high.

An important property of bulk water is the solvation shell coordination number, which can be determined by integrating $g(r)$

$$n(r) = 4\pi\rho \int_{r^\dagger}^{r} r^2 g(r)\, \mathrm{d}r \qquad (4)$$

were $n(r)$ is the coordination number, ρ is the ideal bulk density, and the integration is over a volume slice between the radial distance $r^\dagger$ and r. The main difficulty in determining the water oxygen coordination number from the SCC-DFTB simulations was the lack of distinct density depletions between the solvation shells. This made delineating the first, second, and third solvation shells problematic. However, integrating the apparent first solvation shell for the SCC-DFTB and HBD-SCC-DFTB models yields a coordination number almost twice that of experiment; cf. legend of Figure 1A. These present values are in agreement with previously published SCC-DFTB water simulations and simulations of various semiempirical methods.[29,48] The coordination numbers determined for the SCC-DFTB methods are influenced by the broad density depletion region after the first peak, which overlaps with the beginning of the second solvation shell from the experimental data and CPMD simulations. From this data, it is evident that both SCC-DFTB methods overestimate the number of waters in the first solvation shell, creating a clear overcoordination behavior, followed by a very diffuse and loosely coordinated second shell and essentially no third solvation shell. Taking the coordination numbers and $g_{OO}(r)$ into account, an overall picture of the solvation environment begins to emerge. It is apparent that there are between 2.4 and 3.7 additional waters surrounding a "tagged" central water for the SCC-DFTB and HBD-SCC-DFTB methods. In addition to these oversolvation tendencies, the SCC-DFTB methods have a difficulty in forming distinct second and third solvation shells.

To help visualize the overall 3-D structure of the water from these various methods, iso-density contour plots of the water oxygens and hydrogens were calculated (Figure 2). The iso-density contours reveal that the tail of the first solvation peak for the original SCC-DFTB is due to loosely bound waters encroaching from the lone pair side of the central oxygen. While the densities pertaining to the surrounding waters receiving a hydrogen bond from the central water grow larger, they remain localized. However, the waters donating hydrogen bonds to the central water (lone pair side) have a larger and more delocalized distribution as compared to CPMD simulations, which indicates a lack of overall structure for these particular water molecules. The contour density plots for the HBD-SCC-DFTB simulations have a distinctly different pattern due to the increased ability of this method to model hydrogen bond energies. The incorporation of the hydrogen bonding damping function increases the localized nature of the waters receiving hydrogen bonds from the central water, bringing the results in closer agreement with CPMD data. This is seen in $g_{OO}(r)$ by the increase in the amplitude and narrowing of the first peak. The waters donating hydrogen bonds tend to have a reduced density and an increased localized pattern indicative of structured water but are still less localized than the CPMD waters.

To further analyze the structural properties of the SCC-DFTB and HBD-SCC-DFTB bulk water, $g_{OH}(r)$ and $g_{HH}(r)$ were compared to experimental data and CPMD simulations. Unlike

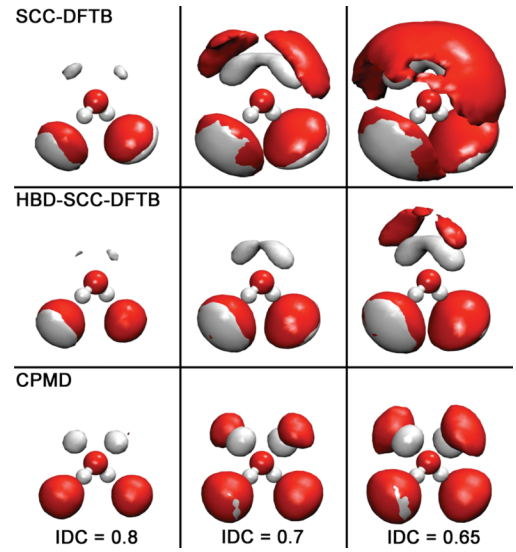

Figure 2. Bulk water iso-density contours for solvating oxygens (red) and hydrogens (white) for the original SCC-DFTB, HBD-SCC-DFTB, and CPMD simulations. Three iso-density contour surfaces (IDC) are presented for each method to clarify the overall 3-D structure.

$g_{OO}(r)$, both $g_{OH}(r)$ (Figure 1B) and $g_{HH}(r)$ (Figure 1C) have distinct maxima and minima in reasonable agreement with experimental data. All models slightly overestimate the position of the second peak of $g_{OH}(r)$ (<0.15 Å) with the CPMD and HBD-SCC-DFTB simulation values being closer to experiment. Only the original SCC-DFTB yields an amplitude close to experiment with CPMD and HBD-SCC-DFTB overestimating the amplitude. This reveals that the original SCC-DFTB may have hydrogen bond lifetimes closer to experiment while the HBD-SCC-DFTB and CPMD methods likely have longer hydrogen bonding lifetimes. The original SCC-DFTB and HBD-SCC-DFTB results poorly reproduce the density depletion between the first and second solvation shell (nonbonded hydrogens) of $g_{OH}(r)$, while all models do reasonably well at describing the third peak and the overall $g_{HH}(r)$.

Integrating the second peak of $g_{OH}(r)$ for all methods reveals an average number of nonbonded hydrogens surrounding the central water in reasonable agreement with experiment, Figure 1B. The HBD-SCC-DFTB method slightly overestimates the experimental value and is higher than the original SCC-DFTB method, indicating that the overcoordination found in $g_{OO}(r)$ is mainly due to the waters donating a hydrogen bond to the central water, which is also confirmed by the iso-density contour plots. The higher amplitude in $g_{OH}(r)$ for the SCC-DFTB models around 2.4 Å (density depletion region for experimental data and CPMD simulations) is due to the presence of the second solvation shell oxygens encroaching on the first solvation shell, predominantly on the lone pair side of the central water, but also from the bonded hydrogen's side, as seen in the iso-density occupancy plots.

3.1.2. Energetic Properties. Evaluation of the water dimer interaction energies of the SCC-DFTB methods as compared to MP2/aug-cc-pV5Z calculations[19] reveals specific deficiencies in the pair interaction that help to explain the anomalies found in the bulk properties (Figure 3). The dimer interaction energies for the original SCC-DFTB method accurately predict the equilibrium dimer interaction distance but overestimate the repulsion energy at short distances while underestimating the stabilization of the dimer at the equilibrium distance. The original SCC-DFTB method also underestimates the stabilization energy at intermediate sepa-

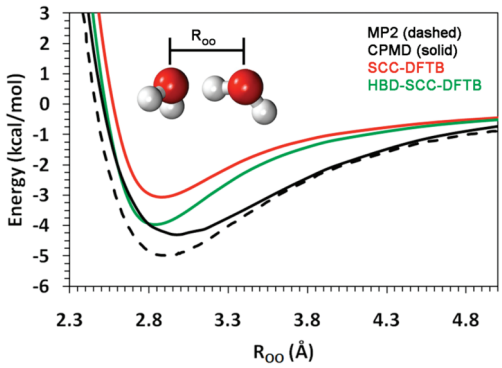

Figure 3. Water dimer interaction energy as a function of the oxygen−oxygen separation distance. Geometries for the energy calculations were taken from ref 19. Results are reported for the original SCC-DFTB (red), HBD-SCC-DFTB (green), CPMD (black solid), and MP2/aug-cc-pV5Z (black dashed) methods.

ration distances (3.3−4.3 Å). The underestimation of the equilibrium dimer energy indicates that the hydrogen bonding energy in the water model is significantly underestimated. This leads to less structured water in the first solvation shell, as shown in the second half of the first peak of $g_{OO}(r)$, the "tail" region of $g_{OO}(r)$, and the increased iso-density contours from the occupancy plots. The underestimated intermediate regions, which correspond to the second solvation shell, result in an under-stabilization of the second solvation shell. The under-stabilized first and second solvation shell results in the lack of an overall tetrahedral structure, as seen in the occupancy data and lack of pronounced density depletions in the various RDFs.

The HBD-SCC-DFTB method more accurately reproduces the short-range repulsive energy and equilibrium dimer interaction energy, although the predicted equilibrium dimer interaction separation is slightly shortened as compared to high level QM calculation (cf. Figure 3). The HBD-SCC-DFTB method also underestimates the stabilization energy in the intermediate regions. The increased ability of the HBD-SCC-DFTB method to model the dimer interaction energies has the effect of narrowing the first peak in $g_{OO}(r)$ and shifting the first peak to a shorter distance, in better agreement with experiment. It is clear that both SCC-DFTB methods underestimate the stabilization energy at intermediate distances. This energy region, however, is accurately reproduced by the HCTH functional CPMD method. The importance of this region on the second solvation shell and the overall structure is apparent in the CPMD simulation's ability to predict the long-range structure properties of water and the inability of the SCC-DFTB method to capture these features.

In addition to the insights that the water dimer interaction energy yields, it is also important to evaluate bulk energetic properties. The heat of vaporization is a quantity that, while directly related to the dimer interaction energy, gives an indication of the whole system interaction energy. The heat of vaporization can be calculated from the MD simulations by utilizing the following relationship:[49]

$$\Delta H_{vap} = -E_{int} + RT \tag{5}$$

where E_{int} is the mean intermolecular interaction energy. The mean intermolecular interaction energy can be calculated by evaluating

$$E_{int} = \frac{\langle E_n \rangle - (n \cdot E_{gas})}{n} \tag{6}$$

where $\langle E_n \rangle$ is the ensemble average potential energy of the interacting water molecules in bulk, E_{gas} is the gas phase energy of a single water molecule, and n is the number of water molecules in the simulation. The original SCC-DFTB and HBD-SCC-DFTB methods both underestimate the heat of vaporization (4.09 ± 0.04 and 7.0 ± 0.08 kcal/mol, respectively) with respect to the experimental value (10.50 kcal/mol). These values, while significantly lower than the experimental value, are in good agreement with the ΔH_{vap} values calculated for the AM1 and PM3 semiempirical methods, 7.69 ± 0.56 and 4.68 ± 0.84 kcal/mol, respectively.[48] The increased accuracy of the HBD-SCC-DFTB's ΔH_{vap} as compared to experiment is due to the increase in stabilization of the water dimer interaction (i.e., its improved description of the hydrogen bonding energy).

3.1.3. Dynamical Properties. The diffusion coefficient is an important dynamical property that indicates the overall fluidity of the solvent. The diffusion coefficient can be calculated by the slope of the mean-square displacement as a function of time according to the Einstein equation:[50]

$$D = \lim_{t \to \infty} \frac{\langle |\mathbf{r}(t) - \mathbf{r}(0)|^2 \rangle}{6t} \tag{7}$$

where $\mathbf{r}(t)$ denotes the position vector at time t and $\langle ... \rangle$ denotes an ensemble average. The experimentally determined oxygen diffusion coefficient for water at 300 K is 0.23 Å^2/ps, Table 1. The oxygen diffusion coefficients for HCTH functional CPMD, original SCC-DFTB, and HBD-SCC-DFTB are 0.1 ± 0.03, 1.11 ± 0.04, and 0.65 ± 0.02 Å^2/ps, respectively. From these results, it is evident that the water in the two SCC-DFTB models diffuses at a significantly elevated level as compared to experiment. The HBD-SCC-DFTB result has a slightly reduced value for diffusion that is due to the increased dimer stabilization energy which results in a more tightly associated first solvation shell and an increase in the ordering of the waters on the lone pair side of the central water. By comparison, the diffusion coefficient for the CPMD simulation is slower than the experimentally determined value due to the tendency for overstructuring of the CPMD water, as seen in $g_{OO}(r)$.

3.2. Hydrated Excess Proton Simulations. The energetic, structural, and dynamical nature of the hydrated excess proton is a fundamental aspect of acid−base chemistry and many biologically important systems. To study this complex (H^+ and associated waters) via computational simulation requires that the underlying computational methodology correctly reproduces

TABLE 1: Diffusion Coefficients

	SCC-DFTB	HBD-SCC-DFTB	CPMD	Exp
H_2O	1.11 ± 0.04 Å^2/ps	0.65 ± 0.02 Å^2/ps	0.1 Å^2/ps	0.23 Å^2/ps[a]
H_3O^+	0.81 ± 0.03 Å^2/ps	0.9 ± 0.2 Å^2/ps	0.33 Å^2/ps	0.94 ± 0.01 Å^2/ps[b]
$D_{hydronium}/D_{water}$	0.73	1.38	3.30	4.09

[a] Reference 57. [b] Reference 66.

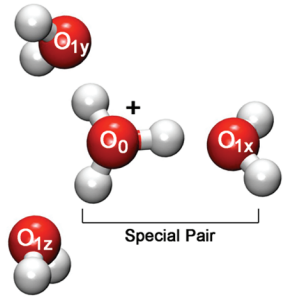

Figure 4. Solvation of the excess proton. The special pair consists of the central hydronium oxygen (O_0) and the nearest water (O_{1x}). The remainder of the complex is composed of O_{1y} and O_{1z} with O_{1y} closer to the hydronium oxygen (O_0) than O_{1z}.

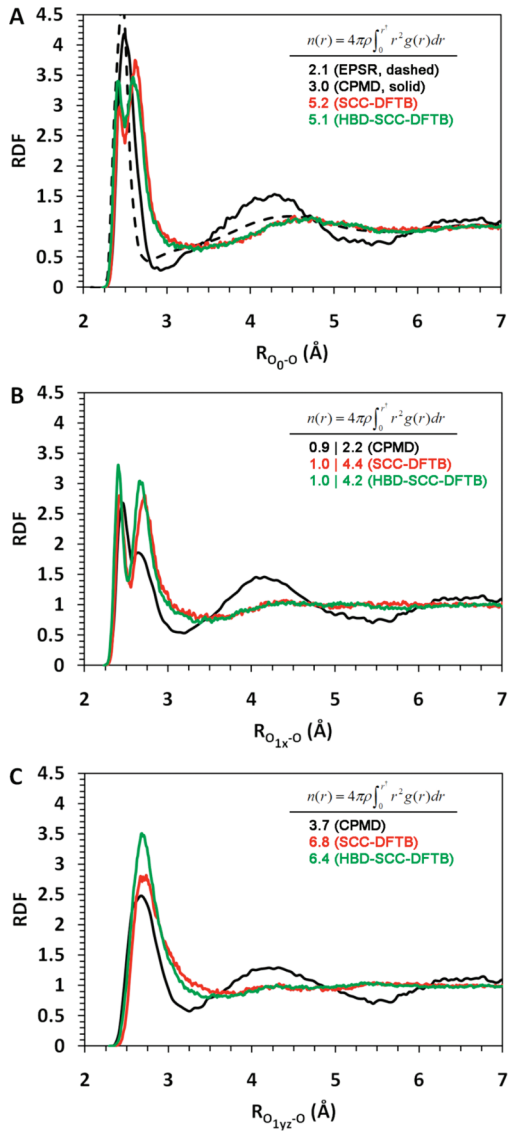

Figure 5. Radial distribution functions of the hydrated excess proton complex for (A) $g_{O_0O}(r)$, (B) $g_{O_{1x}O}(r)$, and (C) $g_{O_{1yz}O}(r)$. Each panel has data for CPMD (black solid), SCC-DFTB (red), and HBD-SCC-DFTB (green) simulations. Panel A also has the experimental EPSR data from refs 51 and 52 (black dashed). The coordination numbers in part A are for the integration of the entire first peak. In parts B and C, the coordination numbers before "|" are from the integration of the first subpeak while the values after "|" are from the integration of the second subpeak.

the inherent delocalized nature of the charge defect as well as its diffusion. Presented here is a systematic analysis of the excess proton in bulk water utilizing the original SCC-DFTB and HBD-SCC-DFTB methodologies. The evaluation of structural properties (RDFs), energetic properties (potential of mean force for proton transfer), and dynamical properties (excess charge diffusion constant and proton hopping characteristics) is compared to empirical potential structure refinement (EPSR) of neutron diffraction data[51,52] and HCTH functional CPMD simulations. From these analyses, the complex interactions of the excess proton with the underlying water model as determined by the SCC-DFTB methodologies are evaluated. It is noted that the neutron diffraction data was collected for highly concentrated HCl solutions and the EPSR method utilized a classical nondissociable model for H_3O^+ (i.e., localized). When appropriate, these limitations and their resulting impact on structural features will be noted.

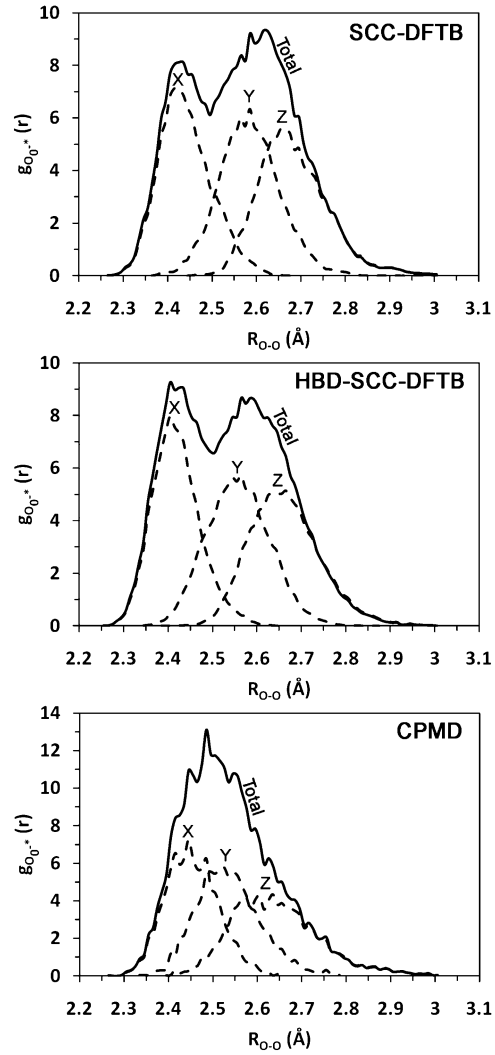

Figure 6. Partial radial distribution functions for the three closest waters to the hydronium oxygen for SCC-DFTB (top), HBD-SCC-DFTB (middle), and CPMD (bottom) simulations. The symbols "X", "Y", and "Z" stand for the O_{1x}, O_{1y}, and O_{1z} waters, respectively.

3.2.1. Structural Properties. For the structural and dynamical analyses, the atoms participating in the solvation of the excess proton are identified as indicated in Figure 4. In Figure 4, O_0 corresponds to the "hydronium" oxygen (the oxygen most closely associated with the excess proton). This oxygen is determined by geometric criteria (oxygen with the nearest three hydrogens); O_{1x} is the "special pair" nearest oxygen to O_0 that is involved in the so-called "special pair dance",[53,54] and O_{1y} and O_{1z} are the other two solvating waters (where O_{1y} is the one closer to O_0 than O_{1z}). This classification of the excess

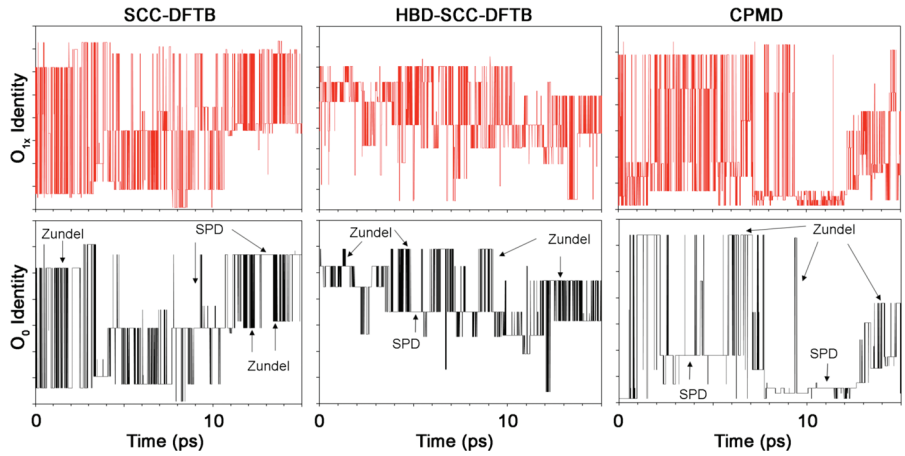

Figure 7. Time dependence of the identity of the special pair partner, O_{1x}, and the hydronium oxygen, O_0, for the SCC-DFTB, HBD-SCC-DFTB, and CPMD simulations. In the top panel, Zundel refers to the Zundel cation and SPD refers to the special pair dance of the Eigen cation. The data depicted here is for one of the two independent trajectories.

proton and associated water molecules allows for a more detailed analysis of the water molecules participating in solvating the excess proton. The two limiting hydrated proton structures are the Eigen cation, $H_9O_4^+$, and the Zundel cation, $H_5O_2^+$.[2,3,55,56]

The result for the RDF of the hydronium oxygen, which describes the overall solvation structure of the hydrated excess proton, is found in Figure 5. From Figure 5, it is clear that both SCC-DFTB models yield a significantly different solvation structure from that seen in the experimental EPSR data[51,52] and from the CPMD simulations. It is noted here that multistate empirical valence bond (MS-EVB) simulations also generally agree with the experimental and CPMD results.[3,31,57] One major difference in the SCC-DFTB results is the bimodal distribution in the first peak of $g_{O_0O}(r)$, Figure 5A. This structural feature is typical of the Zundel cation with the first subpeak indicating the special pair partner (O_{1x}) and the second subpeak representing the other solvating waters in the first solvation shell (O_{1y} and O_{1z}), which can be seen in the partial RDF for the three closest waters to the hydronium oxygen, Figure 6.[53]

The O_{1x} distribution in the bimodal first peak reveals that the original SCC-DFTB method simulations predict a shorter average O_0-O_{1x} separation than the CPMD simulations, Figures 5B and 6. This reduction in the special pair separation is further contracted in the HBD-SCC-DFTB simulations. In addition to the shorter special pair distance, the O_{1y} and O_{1z} separation distances increase, forming a distinct solvation structure around O_0 with relatively less identity switching between O_{1x} and O_{1yz}, as seen by the density distributions in Figure 6. This prominent Zundel character is not seen in the experimental EPSR data or in the CPMD simulations where there is an appreciable amount of Eigen cation character and swapping of the first solvation shell special pair identity (or "rattling") typical of the special pair dance.[53,54,58] The dynamical movement in the special pair dance as seen in the CPMD simulations presented here and in refs 52 and 53 requires significant overlap of the O_{1x} and O_{1yz} distributions as the special pair switches between the three hydronium solvating waters. This process is present to a much lesser extent in the SCC-DFTB simulations, which are dominated by the Zundel cation with fewer switches of the special pair partner among the solvation waters, cf. Figure 7.

In addition to the bimodal distribution, the back half of the first RDF peak and the first density depletion region appear to suffer from the same issues as the underlying SCC-DFTB water structure. More specifically, the first peak is broader (due to the back half of the first peak), the first density depletion region is at a larger separation distance, the density depletion region is broader, and the amplitude of the density depletion region is higher compared to the experimental EPSR data and CPMD simulations. The $g_{O_0O}(r)$ values for both of the SCC-DFTB simulations beyond 4 Å are in good agreement with EPSR data, but they miss the density depletion region below 3 Å and the shoulder region between 3 and 4 Å. Both of the SCC-DFTB simulations appear to reproduce the amplitude and position of the second peak of the EPSR data, while the CPMD simulations predict too short of a separation distance and overestimate the amplitude, which may be attributed to the concentrated acid solution used in the experiments. It also is noted that the EPSR data may result in a higher amplitude of the first peak, a shorter separation distance for the first peak, and a somewhat shifted first density depletion due to the use of a nondissociable localized classical H_3O^+ model in the experimental data inversion.[57]

Integrating the first peak in $g_{O_0O}(r)$, which indicates the number of waters solvating the hydronium oxygen, reveals an oversolvation of the hydronium oxygen of two to three waters for the original SCC-DFTB and HBD-SCC-DFTB methods as compared to CPMD simulations and EPSR data, cf. Figure 5A. The coordination numbers for the SCC-DFTB methods thereby indicate an oversolvation of the hydronium oxygen (O_0), with the additional water density primarily due to additional solvation on the lone pair side of the hydronium oxygen. Unlike the case for the underlying water $g_{OO}(r)$, the HBD-SCC-DFTB method does not seem to improve upon the structural characteristics of the original SCC-DFTB for the hydrated excess proton.

Calculating the RDFs for O_{1x} and O_{1yz} yields additional information on the fine structure of the excess proton complex. It is evident that for both SCC-DFTB methods the first subpeak of $g_{O_0O}(r)$ is due to the O_{1x} water oxygen, as seen by the overlap of the $g_{O_0O}(r)$ and $g_{O_{1x}O}(r)$ distributions, the coordination number of 1 for both peaks, and the partial RDFs. $g_{O_{1x}O}(r)$ for both the CPMD and SCC-DFTB models possess a bimodal distribution with the SCC-DFTB models having more pronounced first and second peaks, indicting a more rigid Zundel structure as compared to the CPMD simulations. Due to the increased Zundel cation character in the SCC-DFTB models, the second peak of $g_{O_{1x}O}(r)$ has an elevated amplitude and is more defined than in the CPMD model. Inspection of the coordination number for the second peak in $g_{O_{1x}O}(r)$ indicates a greater solvation of the O_{1x} water by two additional waters as compared to CPMD simulations, cf. Figure 5B.

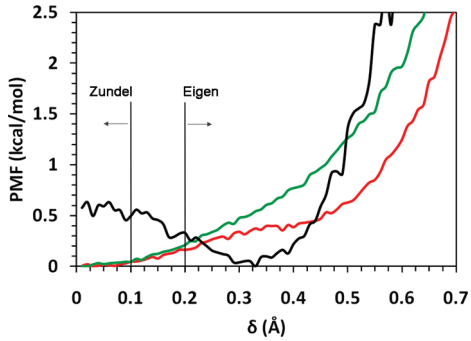

Figure 8. Potential of mean force for the hydrated excess proton for the SCC-DFTB (red), HBD-SCC-DFTB (green), and CPMD (black) methods. The potential of mean force is represented as a function of the δ coordinate, eq 9. The Zundel cation corresponds to $\delta \leq 0.1$, while the Eigen cation corresponds to $\delta \geq 0.2$.

Overall, the SCC-DFTB results are significantly different than the CPMD simulations and the experimental data, which indicate a distorted Eigen cation with one dynamically changing special partner (coordination number from first peak in $g_{O_{1x}O}(r)$), and with the special partner (O_{1x}) being solvated on average by two other waters. Unlike $g_{O_{1x}O}(r)$, the $g_{O_{1yz}O}(r)$ results for both the SCC-DFTB and CPMD simulations appear to be similar, with the SCC-DFTB simulations indicating a higher amplitude and coordination number, again indicative of the oversolvation tendencies of the SCC-DFTB method, as seen in Figure 5C. When evaluating the differences between the original SCC-DFTB and HBD-SCC-DFTB models, it is clear that the HBD term increases the Zundel character of the hydrated proton charge defect, as seen by the elevated first peak in $g_{O_0O}(r)$ and $g_{O_{1x}O}(r)$, Figure 5A,B. This structural change represents a stabilization of the special pair relative to the O_{1y} and O_{1z} waters, although there is no significant impact on the corresponding coordination numbers.

3.2.2. Energetic Properties. The potential of mean force (PMF) for the proton transfer event is representative of the overall contributions of many body and entropic effects in the solution phase. In addition, the integration of the PMF reveals the probability of forming either the Eigen or Zundel cation

$$P_{\text{Eigen|Zundel}} = \frac{\int_a^b e^{-\beta F(\delta)}\, d\delta}{\int_0^\infty e^{-\beta F(\delta)}\, d\delta} \tag{8}$$

where P is the probability, δ is the reaction coordinate, a and b represent the subset range, and $F(\delta)$ is the free energy. The identification of the Zundel or Eigen cation character can be determined by a geometric criteria, given by

$$\delta = |\vec{r}_{O_0H} - \vec{r}_{O_{1x}H}| \tag{9}$$

where $\delta \geq 0.2$ corresponds to a (distorted) Eigen cation and $\delta \leq 0.1$ corresponds to a (nearly symmetric) Zundel cation, as described in ref 53. The free energy of the proton transfer event in bulk water for the SCC-DFTB, HBD-SCC-DFTB, and CPMD simulations is found in Figure 8. From Figure 8, it is clear that the CPMD and SCC-DFTB simulations yield very different results. The CPMD simulations yield a well around the minima at $\delta = 0.325$ corresponding to the Eigen species and a somewhat ($\leq$0.5 kcal/mol) unfavorable free energy for the Zundel species. This CPMD PMF indicates a dynamical system where the character of the excess proton changes between the Eigen and Zundel species with a clear preference for the Eigen species,[53,54] a finding that is consistent with the MS-EVB model.[31,57] These results also suggest that the distorted Eigen species is the "resting state" of the excess proton with the Zundel species occupying the role as the transition state for proton transport, which has been supported by photoelectron spectroscopy.[59,60] These results, described in ref 53, support the Eigen−Zundel−Eigen transition mechanism[56,61] for proton transport. In contrast, the simulations using the original SCC-DFTB method yield just the opposite behavior, i.e., a minimum in the Zundel region and an unfavorable free energy for the Eigen species, which results in a Zundel−Zundel mechanism[62−64] for proton transport in the SCC-DFTB methodology (and at odds with the results of CPMD and MS-EVB simulations). Upon integration, it is found that the SCC-DFTB simulations predict a much more strongly distorted (almost a Zundel cation) Eigen species and an appreciable amount of almost purely symmetric Zundel character, which is reflected in the hydronium oxygen RDFs. The incorporation of the HBD term apparently stabilizes the Zundel region even more and eliminates the weak plateau in the distorted Eigen region seen in the SCC-DFTB PMF. Thus, both SCC-DFTB methods, in contrast to CPMD, provide a Zundel−Zundel type mechanism for proton transport instead of an Eigen−Zundel−Eigen mechanism. Recent CPMD results using a more highly converged basis set have further supported the latter mechanism.[53,54,57,58]

3.2.3. Dynamical Properties. In addition to the structural and energetic features of the hydrated excess proton, the dynamical properties such as the charge defect diffusion coefficient and hopping rate are important in determining how the excess proton is transported through the water hydrogen bonding network. In particular, the ratio of the diffusion coefficient for the charge defect hydronium oxygen and the underlying water oxygens ($D_{\text{hydronium}}/D_{\text{water}}$) is an important quantity that highlights the level of diffusion enhanced by the Grotthuss hopping mechanism[56,65] compared to the standard classical translational diffusion process. The hydronium oxygen diffusion coefficients for the SCC-DFTB, HBD-SCC-DFTB, and CPMD simulations are shown in Table 1. The values of the hydronium oxygen diffusion coefficients for the SCC-DFTB and HBD-SCC-DFTB simulations are quite similar to the underlying water model, with ratios of 0.73 and 1.38, respectively. These results are inconsistent with the experimental data[66] and CPMD simulations, which indicate a larger Grotthuss component with ratios of 4.09 and 3.3, respectively. It should also be noted that the SCC-DFTB pure water diffusion constants are a factor of 3 to 4 above the experimental value.

To gain greater insight into the mechanism for proton transport in the SCC-DFTB and CPMD simulations, the hydronium oxygen's identity was followed during the simulation, cf. Figure 7. The time evolution of the O_0 index and the special pair partner index, O_{1x}, appear to be similar between the SCC-DFTB and CPMD simulations. Both simulations possess the thick vertical dark regions indicative of rapid proton exchange between two special pair oxygens, i.e., the Zundel species, and the thinner line regions depicting the more localized distorted Eigen species. Upon closer inspection of Figure 7, it is seen that the SCC-DFTB simulations contain a greater quantity of thick bar regions than those in the CPMD simulation. The more abundant dark regions reveal an increased Zundel nature in the SCC-DFTB simulations. These results are not surprising given the stabilized wells around the Zundel ion in the SCC-DFTB and HBD-SCC-DFTB PMFs (Figure 8).

To delve further into the dynamics of the proton transfer behavior, the rate of the Grotthuss shuttling and the overall

proton hopping rate need to be calculated. The Grotthuss shuttling rate, also called the *forward hop* rate, is calculated by the accumulation function:[57]

$$\begin{aligned} h(\Delta t) &= h(\Delta t - 1) + \Delta h(\Delta t) \\ h(0) &= 0 \end{aligned} \tag{10}$$

where Δt is the time step and $\Delta h(\Delta t)$ is evaluated as follows:

$$\Delta h(\Delta t) = \begin{cases} 0, \text{if no proton hop } (O_0 \text{ identity remains unchanged}) \\ 1, \text{if the proton hops to a new donor} \\ -1, \text{if the proton hops to the last donor} \end{cases} \tag{11}$$

Analyzing the proton transport events in this fashion allows for the identification of the two main types of hopping events: the *oscillatory shuttling* and the *Grotthuss shuttling*. The oscillatory shuttling is classified as the back and forth hopping between the hydronium oxygen and its special partner, while the Grotthuss shuttling is classified as a hop such that the subsequent hop takes the hydronium oxygen to a third and new water molecule. The calculated proton hopping dynamics, as defined by the accumulation function, are shown in Figure 9. All simulations appear to have similar Grotthuss shuttling rates and overall proton shuttling rates that are close to the experimental proton shuttling value of 0.71 ps^{-1}, although the mechanisms of proton transport are different (see below).[57] All simulations possess the typical fast subpicosecond oscillatory shuttling indicative of the Zundel species (transient horizontal regions), and the relatively infrequent Grotthuss shuttling events (vertical jumps), Figure 9. An important difference between both the SCC-DFTB simulations and the CPMD simulations is that in both the SCC-DFTB simulations oscillatory shuttling does not last as long as that found in the CPMD simulations. The CPMD simulations have two major oscillatory shuttling stretches of ~10 ps and several shorter stretches that correspond to the relatively long "resting" period of the Eigen cation between Grotthuss shuttling events. The overall lifetimes of these oscillatory shuttling stretches are believed to be dictated by the water network reorganization that enables the excess proton diffusion.[57,67] This reorganization is thought to correspond to the rate-limiting step for proton transport. It is of note that this reorganization is much slower than the individual oscillatory shuttling events but is on the time scale of the larger oscillatory shuttling stretches in the CPMD simulations. This is not the case for either of the SCC-DFTB simulations where the oscillatory shuttling stretches last 3−5 ps for the original SCC-DFTB simulations and are slightly shorter for the HBD-SCC-DFTB simulations. These shorter oscillatory shuttling lifetimes, in addition to the infrequent Grotthuss shuttling events, point to a very different mechanism of proton transport than those in the CPMD simulations. In the SCC-DFTB simulations, the proton scoots along from one Zundel pair to the next Zundel pair with infrequent and relatively short Grotthuss shuttling bursts instead of translocating through several waters in a short burst, as seen in the CPMD simulations (tall vertical regions). The shorter oscillatory shuttling stretches indicate that the rate-limiting hydrogen bonding rearrangement time may be significantly shorter in the SCC-DFTB methods. This shorter hydrogen bonding rearrangement time is likely due to the underrepresentation of the water dimer interaction energy that also results in an elevated bulk water diffusion coefficient. The fast dynamical properties along with the Zundel to Zundel scooting mechanism reveals a different type of proton transport dynamics than that seen for the CPMD or for the MSEVB 3 simulations,[57] which give an Eigen−Zundel−Eigen proton transport mechanism.

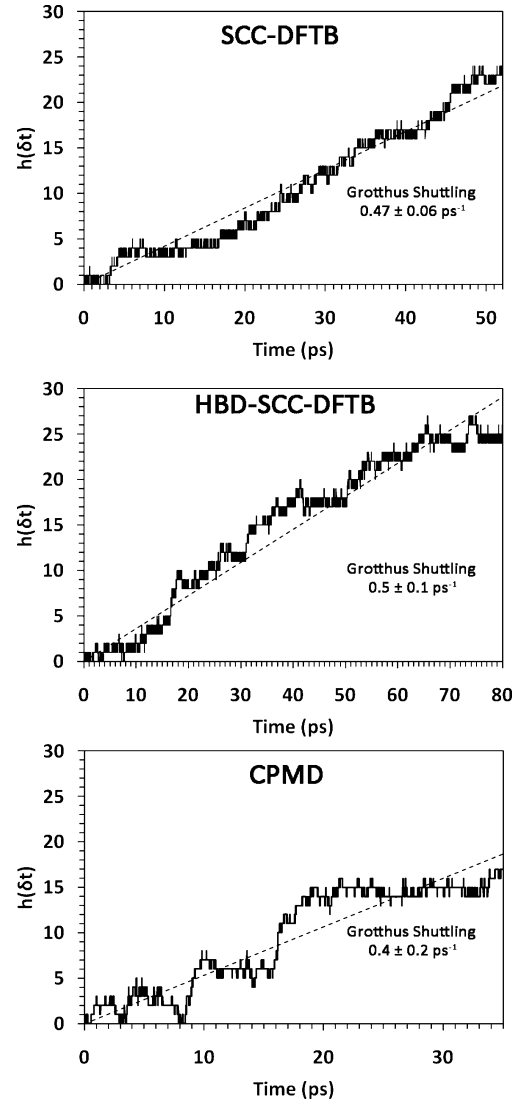

Figure 9. Forward hop function (eq 10) calculated from the SCC-DFTB, HBD-SCC-DFTB, and CPMD simulations. The dashed line indicates the linear best fit to the data that passes through the origin (Grotthuss shuttling rate). The data depicted here is for one of the two independent trajectories, while the average and standard deviations for the Grotthuss shuttling were calculated using both independent trajectories. Note, however, that the mechanism of the shuttling is very different between the SCC-DFTB simulations and the CPMD simulation (see text for additional discussion).

4. Conclusions

Presented in this manuscript is a detailed analysis of bulk water and the hydrated excess proton in water simulations as represented by the SCC-DFTB, HBD-SCC-DFTB, and CPMD methodologies. This analysis reveals that the original SCC-DFTB method predicts an overcoordination of the first solvation shell in bulk water and an overall lack of water structure in the second and third solvation shell. This behavior is, in part, attributed to the understabilization of the water dimer, which also manifests in a water diffusion coefficient that is ~4 times greater than the experimentally measured value. The incorporation of the HBD term, which is thought to provide an increased

ability to model hydrogen bonding, results in a more accurate water dimer interaction and somewhat improved structural properties for bulk water, but a significant overcoordination of the first solvation shell still persists.

Many of the same issues that exist concerning the ability of the SCC-DFTB method to predict the properties of water are also manifested in simulations of the structural, energetic, and dynamical properties of the hydrated excess proton. In the latter case, both of the SCC-DFTB methods predict a significantly overcoordinated first solvation shell. In the first solvation shell, the hydronium oxygen prefers to form a strong interaction with its special pair partner, resulting in an overstabilization of the Zundel species. These structural features result in the two SCC-DFTB models predicting the Zundel species as the "resting state" of the hydrated proton and a Zundel−Zundel mechanism for the proton transport. These results are in contrast to CPMD and MS-EVB simulations, as well as recent experimental work, that suggest the distorted Eigen species as the resting state of the excess proton in water and an Eigen−Zundel−Eigen mechanism for proton transport.

Acknowledgment. This work was supported by the National Science Foundation (CHE-0719522). The authors thank Dr. Sergei Izvekov for the CPMD simulation data, Dr. Tae Hoon Choi for the water dimer and proton transfer geometries, and Drs. Chris Knight and Matt Petersen for helpful discussions.

References and Notes

(1) Car, R.; Parrinello, M. *Phys. Rev. Lett.* **1985**, *55*, 2471.
(2) Marx, D. *ChemPhysChem* **2006**, *7*, 1848.
(3) Swanson, J. M. J.; Maupin, C. M.; Chen, H.; Petersen, M. K.; Xu, J.; Wu, Y.; Voth, G. A. *J. Phys. Chem. B* **2007**, *111*, 4300.
(4) Mackerell, A. D. *J. Comput. Chem.* **2004**, *25*, 1584.
(5) Wang, W.; Donini, O.; Reyes, C. M.; Kollman, P. A. *Annu. Rev. Biophys. Biomol. Struct.* **2001**, *30*, 211.
(6) Xie, W.; Gao, J. *J. Chem. Theory Comput.* **2007**, *3*, 1890.
(7) Song, L.; Han, J.; Lin, Y.; Xie, W.; Gao, J. *J. Phys. Chem. A* **2009**, *113*, 11656.
(8) Elstner, M.; Porezag, D.; Jungnickel, G.; Elsner, J.; Haugk, M.; Frauenheim, T.; Suhai, S.; Seifert, G. *Phys. Rev. B* **1998**, *58*, 7260.
(9) Elstner, M.; Hobza, P.; Frauenheim, T.; Suhai, S.; Kaxiras, E. *J. Chem. Phys.* **2001**, *114*, 5149.
(10) Cui, Q.; Elstner, M.; Kaxiras, E.; Frauenheim, T.; Karplus, M. *J. Phys. Chem. B* **2001**, *105*, 569.
(11) Elstner, M.; Cui, Q.; Munih, P.; Kaxiras, E.; Frauenheim, T.; Karplus, M. *J. Comput. Chem.* **2002**, *24*, 565.
(12) Lin, C. S.; Zhang, R. Q.; Lee, S. T.; Elstner, M.; Frauenheim, T.; Wan, L. J. *J. Phys. Chem. B* **2005**, *109*, 14183.
(13) Krüger, T.; Elstner, M.; Schiffels, P.; Frauenheim, T. *J. Chem. Phys.* **2005**, *122*, 114110.
(14) Zhechkov, L.; Heine, T.; Patchkovskii, S.; Seifert, G.; Duarte, H. A. *J. Chem. Theory Comput.* **2005**, *1*, 841.
(15) Riccardi, D.; Schaefer, P.; Yang, Y.; Yu, H.; Ghosh, N.; Prat-Resina, X.; König, P.; Li, G.; Xu, D.; Guo, H.; Elstner, M.; Cui, Q. *J. Phys. Chem. B* **2006**, *110*, 6458.
(16) Elstner, M. *Theor. Chem. Acc.* **2006**, *116*, 316.
(17) Bohr, H. G.; Jalkanen, K. J.; Elstner, M.; Frimand, K.; Suhai, S. *Chem. Phys.* **1999**, *246*, 13.
(18) Witek, H. A.; Morokuma, K. *J. Comput. Chem.* **2004**, *25*, 1858.
(19) Choi, T. H.; Jordan, K. D. *J. Phys. Chem. B*, DOI: 10.1021/jp912289e.
(20) Smedarchina, Z.; Siebrand, W.; Fernandez-Ramos, A.; Cui, Q. *J. Am. Chem. Soc.* **2003**, *125*, 243.
(21) Schaefer, P.; Riccardi, D.; Cui, Q. *J. Chem. Phys.* **2005**, *123*, 014905.
(22) König, P. H.; Ghosh, N.; Hoffmann, M.; Elstner, M.; Tajkhorshid, E.; Frauenheim, T.; Cui, Q. *J. Phys. Chem. A* **2006**, *110*, 548.
(23) Riccardi, D.; König, P.; Prat-Resina, X.; Yu, H.; Elstner, M.; Frauehneim, T.; Cui, Q. *J. Am. Chem. Soc.* **2006**, *128*, 16302.
(24) Riccardi, D.; König, P.; Guo, H.; Cui, Q. *Biochemistry* **2008**, *47*, 2369.
(25) Riccardi, D.; Cui, Q. *J. Phys. Chem. A* **2007**, *111*, 5703.
(26) Ghosh, N.; Prat-Resina, X.; Gunner, M. R.; Cui, Q. *Biochemistry* **2009**, *48*, 2468.
(27) Hoffmann, M.; Wanko, M.; Strodel, P.; König, P.; Frauenheim, T.; Schulten, K.; Thiel, W.; Tajkhorshid, E.; Elstner, M. *J. Am. Chem. Soc.* **2006**, *128*, 10808.
(28) Phatak, P.; Ghosh, N.; Yu, H.; Cui, Q.; Elstner, M. *Proc. Natl. Acad. Sci. U.S.A.* **2008**, *105*, 19672.
(29) Hu, H.; Lu, Z.; Elstner, M.; Hermans, J.; Yang, W. *J. Phys. Chem. A* **2007**, *111*, 5685.
(30) Gao, J. *J. Chem. Phys.* **1998**, *109*, 2346.
(31) Day, T. J.; Soudackov, A. V.; Cuma, M.; Schmitt, U. W.; Voth, G. A. *J. Chem. Phys.* **2002**, *117*, 5839.
(32) Kast, S. M.; Nicklas, K.; Bär, H.-J.; Brickmann, J. *J. Chem. Phys.* **1994**, *100*, 566.
(33) Hummer, G.; Pratt, L. R.; Garcia, A. E. *J. Phys. Chem.* **1996**, *100*, 1206.
(34) Martyna, G.; Klein, M.; Tuckerman, M. *J. Chem. Phys.* **1992**, 97.
(35) Smith, W.; Forester, T. R. *The DL_POLY_2 User Manual*; CCLRC, Daresbury Laboratory: Daresbury, Warrington, England, 1999.
(36) Aradi, B.; Hourahine, B.; Frauenheim, T *J. Phys. Chem. A* **2007**, *111*, 5678.
(37) Monkhorst, H. J.; Pack, J. D. *Phys. Rev. B* **1976**, *13*, 5188.
(38) Izvekov, S.; Voth, G. A. *J. Chem. Phys.* **2005**, *123*, 044505.
(39) Izvekov, S.; Parrinello, M.; Burnham, C. J.; Voth, G. A. *J. Chem. Phys.* **2004**, *120*, 10896.
(40) Hutter, J.; Ballone, P.; Bernasconi, M.; Focher, P.; Fois, E.; Marx, S. G. D.; Parrinello, M.; Tuckerman, M. CPMD, version 3.5 ed.; copyright IBM Corp. 1990−2001, copyright MPI für Festkorperförschung Stuttgart 1997−2001.
(41) Marx, D.; Hutter, J. *Modern Methods and Algorithms of Quantum Chemistry*; Neumann Institute for Computing: Julich, Germany, 2000; p 301.
(42) Troullier, N.; Martins, J. L. *Phys. Rev. B* **1991**, *43*, 1993.
(43) Boese, A. D.; Doltsinis, N. L.; Handy, N. C.; Sprik, M. *J. Chem. Phys.* **2000**, *112*, 1670.
(44) Kuo, I.-F. W.; Mundy, C. J.; McGrath, M. J.; Siepmann, J. I.; VandeVondele, J.; Sprik, M.; Hutter, J.; Chen, B.; Klein, M. L.; Mohamed, F.; Krack, M.; Parrinello, M. *J. Phys. Chem. B* **2004**, *108*, 12990.
(45) VandeVondele, J.; Mohamed, F.; Krack, M.; Hutter, J.; Sprik, M.; Parrinello, M. *J. Chem. Phys.* **2005**, *112*, 014515.
(46) Grossman, J. C.; Schwegler, E.; Draeger, E. W.; Gygi, F.; Galli, G. *J. Chem. Phys.* **2004**, *1120*, 300.
(47) Soper, A. K.; Benmore, C. J. *Phys. Rev. Lett.* **2008**, *101*, 065502.
(48) Monard, G.; Bernal-Uruchurtu, M. I.; van der Vaart, A.; Merz Jr, K. M.; Ruiz-López, M. F. *J. Phys. Chem. A* **2005**, *109*, 3425.
(49) Fox, T.; Kollman, P. A. *J. Phys. Chem. B* **1998**, *102*, 8070.
(50) Allen, M. P.; Tildesley, D. J. *Computer Simulations of Liquids*; Oxford Science: Oxford, U.K., 1987.
(51) Botti, A.; Bruni, F.; Imberti, S.; Ricci, M. A.; Soper, A. K. *J. Chem. Phys.* **2004**, *121*, 7840.
(52) Botti, A.; Bruni, F.; Ricci, M. A.; Soper, A. K. *J. Chem. Phys.* **2006**, *125*, 14508.
(53) Markovitch, O.; Chen, H.; Izvekov, S.; Paesani, F.; Voth, G. A.; Agmon, N. *J. Phys. Chem. B* **2008**, *112*, 9456.
(54) Swanson, J. M. J.; Simons, J. *J. Phys. Chem. B* **2009**, *113*, 5149.
(55) Tuckerman, M.; Marx, D.; Klein, M. L.; Parrinello, M. *Science* **1997**, *275*, 817.
(56) Agmon, N. *Chem. Phys. Lett.* **1995**, *244*, 456.
(57) Wu, Y.; Chen, H.; Wang, F.; Paesani, F.; Voth, G. A. *J. Phys. Chem. B* **2008**, *112*, 467.
(58) Berkelbach, T. C.; Lee, H.-S.; Tuckerman, M. E. *Phys. Rev. Lett.* **2009**, *103*, 238302.
(59) Winter, B.; Faubel, M.; Hertel, I. V.; Pettenkofer, C.; Bradforth, S. E.; Jagoda-Cwiklik, B.; Cwiklik, L.; Jungwirth, P. *J. Am. Chem. Soc.* **2006**, *128*, 3864.
(60) Kirchner, B. *ChemPhysChem* **2007**, *8*, 41.
(61) Agmon, N.; Goldberg, S. Y. *J. Mol. Liq.* **1995**, *64*, 161.
(62) Kreuer, K.-D.; Paddison, S. J.; Spohr, E.; Schuster, M. *Chem. Rev.* **2004**, *104*, 4637.
(63) Vuilleumier, R.; Borgis, D. *Isr. J. Chem.* **1999**, *39*, 457.
(64) Asthagiri, D.; Pratt, L. R.; Kress, J. D. *Proc. Natl. Acad. Sci. U.S.A.* **2005**, *102*, 6704.
(65) de Grotthuss, C. J. T. *Ann. Chim.* **1806**, *LVIII*, 54.
(66) Roberts, N. K.; Helen, L. N. *J. Chem. Soc., Faraday Trans.* **1974**, *70*, 253.
(67) Lapid, H.; Agmon, N.; Petersen, M. K.; Voth, G. A. *J. Chem. Phys.* **2005**, 14506.

JP1010555